Micromechanics of Fracture Propagation during Multistage Stress Relaxation and Creep in Brittle Rocks

Sana Zafar[1], Ahmadreza Hedayat[1], Omid Moradian[1,2]

[1] Department of Civil and Environmental Engineering, Colorado School of Mines, Golden-80401, Colorado, USA.
[2] Department of Earth Sciences, Swiss Federal Institute of Technology (ETH), Zurich 8092, Switzerland

*Corresponding author: sanazafar@mines.edu, +1 720-329-7962

HIGHLIGHTS

- Fracturing mechanisms under multistage relaxation and creep experiments were identified.
- AE and DIC results showed high evolution of tensile cracks as compared to shear and mixed-mode cracks.
- Frequency-magnitude distribution illustrated a lower *b*-value in case of multistage creep as compared to multistage relaxation.

ABSTRACT

Time-dependent rock deformation caused by the initiation and growth of fractures leads to the weakening of the rock mass. Understanding the fracturing mechanisms involved in the time-dependent behavior in brittle rocks is very important and to achieve this goal, a systematic series of three types of experiments was performed on double-flawed prismatic Barre granite specimens under unconfined compression. The first series aimed to identify the failure mechanism in the short-term failure mode under monotonic loading, the, second series involved multistage relaxation (constant strain) experiments to analyze the damage at different strain levels, and the third series explored the fracture propagation under multistage creep (constant load) experiments. The spatial and temporal evolution of cracking mechanisms were evaluated using the acoustic emission (AE) and two-dimensional digital image correlation (2D-DIC) techniques to observe the whole crack growth process as well as the accumulated inelastic strain at the specified region of interest. Results suggest that in the case of multistage creep experiments, the time to failure was less compared to the multistage relaxation, when loaded above the crack damage threshold (CD) estimated from the monotonic testing. The frequency magnitude distribution of the AE events generated in the three loading conditions followed the Gutenberg Richter model. A relatively lower b-value was obtained for the creep

experiments, indicative of high energy AE events and faster crack growth. In addition, the AE and DIC results also revealed high evolution of tensile cracks at-different stages of creep and relaxation compared to shear and mixed-mode cracks.

KEYWORDS

Brittle rocks, Barre granite, time-dependent failure, multistage stress relaxation, multistage creep, crack mechanisms, tensile and shear cracks.

List of Symbols and Abbreviations	
AE	Acoustic Emissions
BG	Barre granite
CI	Crack Initiation
CD	Crack Damage
LVDT	Linear Variable Differential Transformer
DIC	Digital Image Correlation
UCS	Uniaxial Compressive Strength
ROI	Region of Interest
SEM	Scanning Electron Microscopy
V	Volts
με	Micron-strain
μs	Micron-seconds
ms	Milli-second
dB	Decibels

1. INTRODUCTION

Time-dependent behavior can be described as a phenomenon caused by the weakening of a rock mass with time, such as creep, consolidation/dilation, swelling, and stress relaxation. A detailed knowledge of the time-dependent behavior of rocks is important to predict the long-term stability of underground structures (Diederichs and Kaiser, 1999), surface structures and rock slopes (Kemeny 2005; Yu et al. 2012; Zhang et al. 2020), nuclear waste repositories (Malan et al. 2002; Nara et al. 2010), oil and gas industry, enhanced

geothermal systems (EGS), and CO_2 and waste water disposal (Miura et al. 2003; Zhuang et al. 2020) in which a damage-controlled failure is required.

The behavior of the rock subjected to creep and stress relaxation differs based on the rock type. In brittle rocks, less energy is absorbed, resulting in an abrupt failure as the stress approaches the instantaneous strength of the rock. This behavior is governed by the progressive damage caused by the initiation and propagation of microcracks, which eventually interact and lead to sudden failure. In contrast, ductile rocks absorb more energy and demonstrate visco-elastic behavior when subjected to the stress levels closer to the yield strength (Paraskevopoulou et al. 2018). A large number of experimental and numerical studies have been conducted in the past few decades to analyze the creep and relaxation behavior of soft rocks, such as rock salt or potash in the laboratory under uniaxial, biaxial, and triaxial loading conditions (Yu et al. 2012; Özşen et al. 2014; Mishra and Verma 2015; Cao et al. 2016; Tian et al. 2016; Pramthawee et al. 2017; Yang et al. 2017; Liu et al. 2018; Zhang et al. 2020). However, very few studies have been conducted to analyze the time-dependent behavior in brittle rocks (Hudson and Harrison 1997; Paraskevopoulou et al. 2017; Paraskevopoulou et al. 2018; Wang et al. 2019).

Studies conducted to investigate the long-term strength of brittle rock under constant stress (Bieniawiski et al. 1967; Singh et al. 1975; Schmidtke et al. 1985; Paraskevopoulou et al. 2013; Paraskevopoulou et al. 2018) and constant strain conditions (Peng et al. 1972; Peng 1973; Yu et al. 2012; Tian et al. 2016; Paraskevopoulou et al. 2017; Yang et al. 2017; Liu et al. 2018; Zhang et al. 2020) mostly focused on the mechanical behavior of the rock specimen under time-dependent loading and rarely investigated the damage from a microscopic perspective. Experimental results from creep and relaxation studies were used to introduce constitutive and numerical time-dependent models to predict the long-term strength of the rock (Chugh et al. 1987; Aydan et al. 1996).

In most of these studies, the time-dependent behavior of rock in single-stage and long-term experiments was explored by raising the stress up to a particular level and monitoring the response for longer durations. The results of such studies illuminated different stages of creep and relaxation. The three stages of creep at a constant stress level are termed as the primary, secondary and tertiary creep (Baud et al. 1997). When the applied stress is maintained constant, initially the strain increases with a decreasing strain rate with this stage termed as the primary stage of creep, followed by the secondary creep in which the deformation takes place at a constant strain rate. When the strain rate starts to accelerate towards failure, tertiary creep stage occurs.

To investigate the different stages of relaxation, similar to creep, Paraskevopoulou et al. (2017) conducted relaxation experiments on two types of limestones focusing on the distinct stages of relaxation and the

amount of stress relaxed in these stages at different load levels while holding the axial and radial strains constant. Their results showed similar stress-time responses at different strain levels, revealing three stages of relaxation. The first stage of relaxation was identified as the stage where the stress relaxes with a decreasing rate, due to the evolution of new or pre-existing cracks that initiate during loading with time; this stage is followed by the constant rate of stress drop, known as the secondary stage of relaxation. Once the crack growth stabilizes, no further stress relaxation takes place, i.e., the stress reaches an asymptote, and this stage is referred to as the third stage of relaxation.

These identified mechanisms under creep and relaxation can be observed when the rock is loaded up to a stress level between crack initiation (CI) and crack damage (CD) under single-stage long-term experiments. However, the behavior may differ when the rock is loaded beyond CD. The crack initiation stress threshold (CI) is defined as the first stage of stress-induced damage in low-porosity rocks, indicating the initiation of stable crack growth stage, and this threshold can be used as a lower bound estimate for long-term strength threshold of crystalline rocks (Damjanac and Fairhurst, 2010). However, crack damage (CD) indicates the stress level corresponding to the coalescence of the microcracks and the initiation of unstable crack growth stage (Deiderichs et al. 2004; Nicksiar and Martin 2012).

In practice, the time-dependent deformations under creep and relaxation may occur due to the stress variation in steps in various environmental conditions and engineering applications such as underground excavations, rock slopes, glaciers, and dam abutments. Literature suggests that single-stage creep and relaxation experiments are easier to perform, but consume a large number of samples to analyze the rock response spectrum. However, multistage time-dependent experiments are advantageous to investigate the rock response at target stress levels in a time-efficient manner while avoiding the effect of sample variability (Heap et al. 2009). Cao et al. (2016) conducted multistage and single-stage creep experiments on soft rocks under uniaxial compression. The results of the two loading conditions indicated that the stress level required for creep to occur had a threshold value, below which no creep was observed, with the threshold value independent of the loading condition (i.e., single-stage or multistage). Sabitova et al. (2021) conducted multistage triaxial creep experiments on a set of natural limestone and artificial samples with alternating cycles of creep and stress relaxation. Their results demonstrated that loading and unloading cycles, i.e., creep and stress relaxation, followed different stress-strain laws. At constant stress, during creeping stages of the test, the samples exhibited significant dilation. Similarly, in the case of stress relaxation, despite the constant position of the loading piston, the sample showed slight deformation in the vertical direction during relaxation stages. All of these studies discussed the mechanical properties of rocks during stress relaxation and creep to illustrate the validity and rationality of the constitutive models under investigation. However, the fracturing processes in brittle rocks under relaxation and creep have not been explored in detail.

According to the fracturing processes, the crack (fracture) propagation modes are primarily characterized into three types: mode I (tensile), mode II (in-plane shear) and mode III (off-plane shear or tearing) as reported by Gdoutos (2005), Ko and Kemeny (2007) and Ghazvinian et al. (2013). Depending upon the mode of displacement, cracks can be classified into any of the mentioned types or a combination of them, known as mixed-mode cracks. Hence, the objective of the present study is to examine the response of low porosity brittle rocks under multistage relaxation and creep in terms of spatio-temporal evolution of the microcracks.

AE sensing is a continuous measurement technique used for damage detection in rocks and characterizing the failure mechanisms in rock fracture experiments (Qu et al. 2022). Digital image correlation (DIC) is also the most widely used non-contact optical technique for full-field displacement and strain measurements in real time by comparing the digital images in undeformed and deformed states (Sutton et al. 2009; Hedayat et al. 2014; Shirole et al. 2019). 2D DIC measures in-plane displacements and strains on planar objects and 3D DIC can measure the full-field displacement and strain fields on non-planar objects (e.g., Munoz et al. 2016; Munoz and Taheri 2018). In this study, 2D DIC technique in combination with acoustic emission (AE) were used to analyze the micro and meso mechanism of damage evolution in double flawed prismatic Barre granite specimens under different loading conditions.

The study focused on three different sets of experiments: (1) monotonic uniaxial experiments (2) multistage creep experiments, and (3) multistage relaxation experiments. The monotonic uniaxial experiments were conducted as a baseline testing to determine the damage thresholds CI, CD, and the peak strength (UCS) for the rock specimen and design the procedure for multistage longer-term experiments accordingly. The samples were loaded up to stresses close to its short-term peak stress (above CD) under creep and relaxation to compare the fracturing processes in multistage relaxation and creep experiments with that of monotonic loading experiments.

2. LABORATORY TESTING PROGRAM AND METHODS

2.1 Material

To characterize the damage processes under multistage relaxation and creep, double-flawed Barre granite (BG) specimens were used in this study. BG, which is crystalline in nature, was obtained from the southwest region of Burlington, Vermont (USA). BG is a gray granodiorite with its grain size ranging from 0.2 mm to 3.0 mm (medium-fine grained). It has an average grain size of 0.87 mm (Iqbal and Mohanty 2007; Nasseri et al. 2010). BG composition consists of about 65% feldspar (average grain size of 0.95), 27% quartz

(average grain size of 0.94 mm), and 9% biotite (average grain size of 0.83 mm) (Iqbal and Mohanty 2007; Dai and Xia 2010; Nasseri et al. 2010). It has a density of 2.66 g/cm^3 with a porosity of 0.59% (Iqbal and Mohanty 2007). Intact BG specimens have the following average properties: Young's modulus=58 GPa (Shirole, Walton, and Hedayat 2020), uniaxial compressive strength=170 MPa (Zafar et al. 2020), and average compressional P-wave velocity= 4100 m/s. The same block of Barre granite was used to prepare the prismatic specimens (152 mm x 76 mm x 25 mm) and the pre-existing flaws were cut by an OMAX water jet, through out the thickness of the specimen. The flaw length and inclination angle with respect to the horizontal axis were 12.5 mm and 60°, respectively (Figure 1b).

2.2 Testing Procedure

Multistage relaxation and creep experiments were conducted on a computer-controlled servo-hydraulic loading machine. The loading machine has the capability to operate either in axial-displacement control mode or axial-load control mode. Uniaxial loading was applied in displacement-controlled mode at a constant displacement rate of 1 μm/s for the relaxation experiments. The axial loading system was programmed to apply the load at a constant rate up to the desired stress level and then maintain the displacement for the relaxation experiment. The variation in the displacement during the relaxation period was ± 0.01%. Three linear variable differential transformers (LVDTs) recorded the overall axial deformation of the rock specimens. For the creep experiments, the loading was applied in the load-controlled mode at a constant loading rate of 0.55 kN/s up to the desired stress level at different stages and then the load was maintained constant for the resting period. The duration for the long-term testing was about six hours.

The specimens were instrumented with 12 piezoelectric Nano 30 AE sensors from MISTRAS Group, Inc., which were mounted on the sides of the specimen (Figure 1b). The Nano-30 AE sensor has a frequency response over the range of 125-750 kHz with a resonant frequency of 300 kHz. They were attached on the sides along the longitudinal axis of the specimen with Hardman epoxy (Royal Adhesives and Sealants). Prior to the application of the epoxy, the sides of the specimen were covered with a plastic film to prevent the penetration of the epoxy into the rock pores (Goncalves 2019). The epoxy was in contact with the sensors for nine hours, and the velocity was measured using the pencil lead break (PLB) test, which was documented every 90 minutes for nine hours. The efficiency of the coupling was verified by the PLB test and the auto sensor test (AST).

AE sensors were connected to 2/4/6 PAC preamplifiers to amplify their output voltage by 20 dB and therefore improve the detection efficiency of the sensors for recording. The sampling frequency was 5 MHz with a sample length of 15k and a pre-trigger of 256 μs. A 16-channel board and system from the MISTRAS

Group, Inc. was used as a part of the AE data acquisition system. The system was controlled by *AEwin* real-time operating software where the peak definition time (PDT), hit definition time (HDT), and hit lockout time (HLT) were set as 200, 800, and 350 μs, respectively. The maximum duration was 99 ms. The threshold for these experiments was set as 55dB.

To measure the strain profile at the region of interest, i.e., area around the flaw tips and the bridging region between them, 2D DIC technique was utilized with the application in three stages (Figure 1a): (1) specimen preparation and camera set-up, (2) image acquisition, and (3) image processing using VIC-2D software. A Grasshopper (Point Grey) charged coupled device (CCD) camera with a Fujinon lens having a 35mm focal length was used for image acquisition. The planar surfaces of the specimens were painted with a multi-color paint (Rust-Oleum) to generate random speckle pattern. Proper synchronization was ensured among the three systems during the test.

3. RESULTS

3.1 Mechanical Behavior of Barre Granite Specimens

The average values of UCS, CI, and CD for the Barre granite rock obtained from a series of unconfined compression experiments were 153 MPa, 56 MPa, and 120 MPa, respectively (Figure 2). Based on the results obtained through the monotonic uniaxial experiments, five stress levels (Figure 2a) were selected for the multistage relaxation and creep experiments. The five levels of stress for multistage loading (both relaxation and creep) were set as 40%, 60%, 70%, 80%, and 85% of the UCS ("a" through "e" in Figure 2) and the hold time at each step was constant for all the specimens and equal to ½ hr, ½ hr, 1 hr, 1 hr, and 3 hrs, respectively.

A stepwise loading method was used for the long-term (6 hrs) testing (Figures 2c & 2e) to detect the degree of damage at different stress levels. At the beginning of each test, the specimen was loaded monotonically up to the 40% of the UCS. It was observed that the specimen under multistage creep failed after about 30 minutes of resting time at 85% stress level, while those under relaxation failed after about 2.5 hrs of relaxation at the same stress level. The duration of six hours was selected for the long-term testing, due to operational limitation of the loading machine and the observations of the rock behavior at different stress levels under creep and relaxation modes. During the long-term testing, the overall temperature and humidity conditions were monitored and maintained in the laboratory.

In case of multistage relaxation, at each stress level, the strain was held constant and the damage occurred in the rock, which caused a stress decline in the specimens. Figure 2(c & d) indicates stress relaxation, which occurred from the CI stress level and stayed in the stable crack growth phase. Cracks initiated and

propagated in the relaxation phase, the development of cracks provided free surface for the stress to relax (Paraskevopoulou et al. 2017) and stabilizes the stress after a certain period of time. Initially at stages (a) and (b), which corresponded to stress levels of 40% to 60% of UCS, a smaller amount of stress relaxation occurred, which was a consistent finding for all three rock specimens. With further increases in the level of constant strain (stages c, d, & e), the amount of stress relaxation increased, indicating the extent of the cumulative damage in the rock specimen (Tian et al. 2016). However, due to BG's low porosity and high strength, less stress relaxation occurred compared to sedimentary rocks. It was also observed that, in each relaxation stage, the rate of stress relaxation was higher at the beginning and decreased gradually with time. Due to the operational time limitation of the loading machine, the specimens did not relax completely and hence, the three stages of relaxation as observed in few other studies (Paraskevopoulou et al. 2017; Li and Xia 2000) were not observed. At the final stage (e) in which 85% of the UCS was applied, the specimen failed after approximately 2.5-3 hours of stress adjustment but the failure did not result in catastrophic failure of the specimen.

In case of multistage creep experiments, at each stress level the load was maintained constant for a given duration of time. As the loading time increased, the axial strain increased (Figures 2e & 2f); however, the accumulated damage was less due to machine operation constraints. The specimen showed slight increment in the axial strain at lower stress levels ('a' to 'd') and failed at 85% stress level after 30 minutes, as seen by the upward concave shape of strain in stage (e).

It has been reported in the literature (Paraskevopoulou et al. 2018; Innocente et al. 2021) that in case of brittle rocks, when the applied stress is above or close to the CD of the rock specimen, secondary stage of creep is skipped and accelerated creep rates occur, leading to the failure of the specimen within minutes to hours. In the subsequent sections of this study, the extent of damage at each stage, formation of new microcracks and their mode of deformation, which ultimately impact the failure strength of the rock, are discussed in detail through the registered AE and strain variations.

3.2 Cracking Levels

The onset of cracking (CI) and the beginning of crack interaction and coalescence (CD) were obtained through AE event parameters (Eberhardt 1998; Nicksiar and Martin 2013; Ghazvinian 2015, Moradian et al. 2016) and 2D-DIC strain measurements (Shirole et al. 2020; Zafar et al. 2022). Figure 3 (a & b) shows the CI and CD levels obtained for the monotonic loading experiments.

As shown in Figure 3a, evolution of high amplitude AE events can be observed corresponding to 30-40% of the UCS and a subsequent increase in the event amplitude can be seen around 75-80% of the UCS. Similarly, in Figure 3b, the cumulative AE event plot indicated a change in the slope at around 30-40% of UCS. The initiation in the AE event rate was associated with the CI in the rock specimens. As the stress was further increased above the CI, an accelerated increase in the rate of AE events was seen at around 75 to 80% of the peak strength, indicating the formation of macrocracks that were linked to the CD stress threshold.

To perform a quantitative comparison of the AE events produced in the multistage loading experiments with the monotonic results, the evolution of the AE events and its amplitude were also plotted as a function of time and normalized stress (normalized by the short-term failure stress) for relaxation and creep (Figure 3). Each AE event indicates a microcrack that reflects the damage in the rock specimen (Sassinek et al. 2014). In case of relaxation, as the stress level increased, the stress decay also increased, which gave rise to the number of AE events generated in each stage of relaxation. Since the relaxation stages started above the CI, the evolution of AE events was not only seen in the loading period but also in the relaxation stages, especially at the higher stress levels (60% of UCS and above).

The results showed that at low stress levels of relaxation (stages ‘a’ & ‘b’), very few AE events were generated and the event rate also was lower (Figure 3d). As the stress level approached the peak strength of the rock specimen, the event rate and the cumulative events exhibited an increasing trend even in the relaxation periods. However, at a particular stage of relaxation, the rate of events was higher at the beginning and then decreased gradually with time during the constant strain period, showing the stabilization of the cracks or steady stage (Patel 2017; Li and Xia 2000). Figure 3c illustrates high number of comparatively small amplitude AE events generated in the relaxation experiment. However, few high magnitude events can be observed at 85% relaxation period.

In case of multistage creep experiments, the amplitudes of the AE events were higher (Figure 3e) as compared to the relaxation and monotonic testing results. The high amplitude events were mostly generated in the loading period, while the amplitude reduced in the creep period except stage ‘e’, indicating the evolution of relatively low energy events as the time progressed with constant load. In the last stage of creep (i.e., 85% of UCS), a large number of high amplitude events continuously evolved, representing crack interaction and failure. Amplitudes of the AE events produced in the rock specimen under monotonic loading were expected to be higher than the recorded values due to the faster crack growth and the most likely cause of this observation is the typical saturation of the AE systems due to which high amplitude AE events were clipped and not registered properly by the AE acquisition system. In contrast, in the case of

relaxation and creep experiments, this potential saturation did not occur due to the smaller loading rate. For the sake of better comparison, and avoiding the problem of amplitude distortion due to clipping, wherever needed, we have only shown the results of the monotonic test up to 85% of UCS which corresponds to the stress level in which specimens failed under multistage relaxation and creep.

The high AE event rate and cumulative events plot illustrated high evolution of microcracks in case of creep (Figure 3f). At each stage of creep, the rate of AE event was higher at the time of loading and then decreased under constant creep stress except stage 'e' in which the failure occurred. Particularly, the AE event rate and the amplitude of the events reduced with time at each stress level except 'e' and this can be an indicative of primary and secondary creep stages, where deformation in the rock specimen took place at a decelerating and constant strain rate, respectively. More than 10,000 AE events were recorded in the creep experiments, which was approximately 2.5 times the number of AEs in the relaxation experiments.

Figure 4 demonstrates the crack evolution process for monotonic, relaxation and creep testing on the basis of the total volumetric strain (ε_V) profile of the rock specimen in the specific region of interest (ROI). The total volumetric strain (ε_V) for a sample subjected to axial loading, with or without a confining pressure, and under small strains, is given by the following expression (Martin and Chandler 1994):

$$\varepsilon_V = \varepsilon_A + 2\varepsilon_L \quad (1)$$

where ε_A and ε_L represent the axial and lateral strain magnitudes respectively obtained from the 2D-DIC technique. Figure 4 illustrates the variation of ε_V obtained through DIC corresponding to the CI and CD stress levels for the monotonic, multistage relaxation and creep experiments (Figure 4 a, c & e) The volumetric strain curve deviated from linearity (elastic deformation) at 40% stress level, marking the initiation of microcracking. The axial stress level where the total volumetric strain reversal occurred marks the onset of unstable crack growth (CD), as suggested by Beniawiski (1967). Figure 4b shows the total volumetric strain reversal at around 78% of the peak strength (i.e., the CD stress threshold for the monotonic loading tests). However, the total volumetric strain profile for multistage relaxation experiments exhibited a strain reversal at 60-70% of the peak strength (Figure 4d) which corresponds to the CD (Martin 1994; Diederichs 2004) stress level for the relaxation experiments. In case of creep experiments, it is further lowered to 60% stress level (Figure 4f), due to high increase in the lateral strain as compared to the axial strain (Table 1). This analysis demonstrates higher damage accumulation at a lower stress level in case of creep led to the failure of the specimen in a shorter duration of time at stage 'e'.

The reduced values of the CD and UCS in the case of multistage loading experiments indicated that during the relaxation and creep tests and at various stages, the internal structure of the rock sustained damage due

to the initiation of new cracks. However, the reduction in strength for BG was less pronounced as compared to other sedimentary rocks such as claystone and sandstone (Li and Xia 2000, Tian et al. 2016), which elucidates the less viscous property of this brittle rock.

3.3 Crack locations

To characterize the damage process in the ROI for both the monotonic testing and the longer-term experiments, the spatial structure of the AE sources (located with an accuracy of ± 2mm) in combination with the strain map of the minor principal strain ($\varepsilon_{22;}$ negative (-) strains represent tension) were represented in Figures 5 and 6, respectively. Because tensile damage is the primary mode of deformation in brittle rocks (Diederichs 1999), ε_{22} strain field was specifically chosen to analyze the effect of microcracking in both the loading conditions (Shirole et al. 2019; Shirole et al. 2020; Zafar et al. 2022). According to the AE source location and source type characterization technique developed in Li et al. (2019), the AE source localization and their modes of deformation were identified for the experiments.

Figure 5 shows the AE sources decomposed into their modes of deformation as tensile, shear and mixed for monotonic, relaxation and creep experiments. This type of AE source classification and comparison in case of multistage creep and relaxation is unprecedented in previous research (Heap et al. 2008; Brantut et al. 2013; Paraskevopoulou et al. 2017, 2018). As illustrated in Figure 5a, during the monotonic loading, the clustering of the microcracks around the failure plane took place at 80% of UCS and higher. However, in case of relaxation and creep, the source localization along the actual failure plane took place at a lower stress level (at 70% of UCS for relaxation and 60% of UCS for creep). The fracture pattern became more complex in the creep and relaxation experiments, as compared to the monotonic.

In the case of relaxation, a total of 4,033 AE events were recorded, which was approximately three times the events recorded during the monotonic uniaxial experiments. It is also evident from Figure 5b that the increase in AE activity mostly occurred in the relaxation period at 85% of UCS level. The increase in the number of AE events at each stage of relaxation provided independent evidence for the creation and growth of new cracks, which indicated the accumulated damage along the weaker plane that caused the failure of the rock specimens. A cluster of AE events started to concentrate along the bridging area at 70% of the UCS. The AE cluster became denser in the bridging area (the rock bridge between the two flaws) at 85% of UCS for the relaxation experiments, showing an accumulated damage zone as compared to the same stress level for the monotonic loading experiments (Figure 5a).

During multistage creep experiments (Figure 5c), at lower levels of stress, the AE sources were distributed mostly at the top and bottom of the ROI. As the creep progressed, more AE events were generated and

localized at the center of the specimen. The fracture pattern became more complex, resulting in crack coalescence at a lower stress level (60% of UCS), compared to the relaxation and monotonic results. As the load increased, the cracks covered the entire ROI with a higher crack density along the macroscopic failure plane. Finally, considering all stages of creep together, a complete AE source concentration was observed along the macroscopic fault plane near failure.

To further investigate the damage accumulation during multistage loading experiments, DIC strain profiles were investigated. Figure 6 shows the damage at stress levels corresponding to the five stages of relaxation and creep, represented as strain localization in the ε_{22} strain-field. Figure 6a shows the extensile strain variation for monotonic testing, in which the strain concentration can be seen around the flaw tips at around 80% of the UCS which then further propagated towards the specimen boundaries. However, in case of relaxation and creep, the strain concentration at the flaw tips were seen at 70% and 60% of the UCS, respectively. The DIC results agree with the AE observations and illustrate the evolution of damage zones at lower stress level for relaxation and creep experiments. Clearly, the stress level corresponding to crack initiation through AE observation is lower than DIC, because AE accounts for the damage in the volume of the specimen while DIC captures the incurred strains on the surface of the specimen. Moreover, comparing the three loading conditions, ε_{22} strain-field showed sub-vertical strain concentration features parallel to the loading direction, indicating that the tensile mechanism was the dominant cracking mechanism in short term as well as long-term loading conditions.

3.4 Cracking Mechanisms

To further investigate the temporal and spatial evolution of the microcracks at different stages of creep and relaxation in this study, detailed moment tensor analysis (Li et al. 2019) of the AE events was carried out. Figure 7 shows the temporal evolution of the tensile, shear, and mixed mode cracks in the ROI that were obtained through the moment tensor inversion method employed on the AE signals produced in the different sets of experiments. It is evident from Figures 7c and 7e that the tensile cracks started prior to the first stage of loading for relaxation and creep, (i.e., at the CI). However, the evolution of shear cracks occurred at the higher stress levels (at 70% of UCS for relaxation and 60% of UCS for creep).

The experimental results demonstrated the evolution of a high number of tensile cracks in the ROI both during the loading and the resting periods. The ratio of the tensile cracks with respect to the total number of cracks throughout the experiment were approximately 6 to 7 times the ratio of shear and mixed mode cracks. The high number of tensile cracks can be related to the fact that the various stress levels for relaxation and creep initiated after the CI and remained in the stable crack growth stage, which led to the formation of more tensile cracks or the opening of existing cracks. This observation was supported by the

work of Matsushima (1960), who concluded that in case of long-term loading on granitic rocks, the lateral strain caused by the extension of the microcracks was higher than the strain in the longitudinal direction. Hence, tensile induced microcracking is responsible for long-term deformation in crystalline rocks.

Furthermore, with increasing stress levels, shear and mixed mode cracks also evolved. Specifically, comparing the cracking mechanisms in relaxation and creep, it is evident from Figures 7c and 7e, that at stage 'e' (85% stress level) under relaxation, the contribution of the tensile crack is the highest compared to shear and mixed mode cracks. However, at the same stage under creep, all the three types of cracks showed an increasing trend. The distinct changes observed in the AE signatures at different stages of creep and relaxation as the damage progressed in the rock specimens thus proved that the time-dependent behavior of brittle rocks occur due to the formation of new microcracks with a higher contribution of tensile cracks.

To verify the temporal evolution of the cracks obtained through the moment tensor analysis of AEs, the non-elastic tensile (ε_{AT}^{NE}) and non-elastic shear (γ_{AS}^{NE}) strain distribution obtained through 2D-DIC were analyzed in the ROI for all the three loading conditions. The procedure described in Shirole et al. (2020) was adopted for the measurement of the non-elastic tensile (ε_{AT}^{NE}) and shear strain (γ_{AS}^{NE}) components at the pixel scale. Considering the evolution of non-elastic tensile strain as the indicator of the tensile damage and the evolution of non-elastic shear strain as the indicator of shear damage in the rock specimen, the non-elastic tensile and non-elastic shear strains obtained through 2D-DIC were plotted as a function of the time normalized by the time of failure (Figures 7b, 7d & 7f).

Figure 7b demonstrates that the tensile damage in the rock specimen occurred around the stress level corresponding to the CI and proliferated with increased damage, which was in close agreement with the AE observations. The non-elastic shear strain field amplified as the stress increased beyond 80% of the UCS. Figures 7d and 7f show that the shear damage in the rock specimen initiated at stage 'c' (70% of UCS) for the long-term experiments. The trends shown by the non-elastic strain metrics were consistent with the AE signatures, further corroborating the fact that the primary mode of deformation in brittle rocks is local tensile cracking caused by the concentration of extensile strain (Lajtai 1974; Tapponier and Brace 1976; Kranz 1983; Moore and Lockner 1995). The ratio of the non-elastic tensile and shear strain in the ROI at different stress levels in the three loading conditions indicated that the amount of non-elastic tensile strain was much higher than the non-elastic shear strain, which was consistent to the observations made through the moment tensor analysis of the localized AE events.

3.5 Frequency-Magnitude Distribution (b-value)

Earthquakes obey power law distribution, which can be approximated by a frequency magnitude distribution (Gutenberg and Richter, 1944; known as G-R model) as:

$$\log N = a - bM, \tag{2}$$

Describing the relationship between the frequency of earthquakes $N(M)$ with magnitudes larger than or equal to M. The parameter b, often termed as the b-value, refers to the relative size distribution (Scholz 2015).

The frequency magnitude distribution (FMD) of the AE events generated in the monotonic, relaxation, and creep experiments were found to follow the Gutenberg Richter relation (G-R law) given for earthquakes. This analysis is used to estimate the b -value which is defined as the log-linear slope of the frequency magnitude distribution (Rao and Lakshmi 2005). The b-value was determined using the maximum likelihood method as the most appropriate measure (Woessner and Weimer 2005):

$$b = \frac{log_{10}(e)}{\left[\langle M\rangle - (M_c - \frac{\Delta M_{bin}}{2})\right]} \tag{3}$$

where $\langle M\rangle$ is the mean magnitude of the sample, M_C is the magnitude of completeness and ΔM_{bin} is the binning width (magnitude interval) of the catalogue.

An important parameter used in the determination of the b-value from the Gutenberg Richter relation is the Magnitude of completeness (M_C) which represents the lowest magnitude at which 100% of the events in a space-time volume are detected (Rydelek and Sack 1989). The maximum curvature (MAXC) approach was used in this study to determine M_C as described by the work of Wyss and Weimer (2000). This method calculates the first derivative of the frequency-magnitude curve and defines the maximum curvature point as the M_C (Woessner and Weimer 2005).

Figure 8 (a, b & c) demonstrates the b-value variations for the events generated in the fracturing experiments (top row). The circles represent the cumulative distribution of the AE events according to their magnitudes. The lines in the plot indicates the Gutenberg Richter model and the arrow points towards the magnitude of completeness (M_C) calculated by the method of maximum curvature (MAXC). Since the magnitude of the AE events for the laboratory rock fracture experiments are divided by 20; ΔM_{bin} is taken as 0.05 for the b-value calculation.

The b-value estimated for the monotonic uniaxial compression is around 1.6, which is greater than the multistage relaxation and creep experiments, the reason behind this is the evolution of low energy events up to 85% UCS which indicates less evolution of damage in the specimen. Comparing the b-value for the AE events in multistage relaxation and creep reveals that the relaxation experiments produced significantly larger b-values. Physically, this means a high proportion of small AE events in case of multistage relaxation experiments as compared to creep. A higher b-value indicates slow crack growth, while a lower b-value indicates faster and more unstable crack growth that result in a high number of large magnitude events (Rao and Lakshmi 2005). In case of creep experiment, a relatively lower b-value was obtained as compared to relaxation, indicating larger magnitude events and higher damage evolution.

The bottom row (Figure 8d, 8e & 8f) illustrates the spatial variation of the events generated in the different loading conditions along with their amplitudes. The plots for multistage relaxation and creep illustrates that the damage zone was highly populated with low magnitude AE events in case of relaxation, however, relatively large number of higher magnitude events are visible under creep. Lower amplitude and smaller number of events for monotonic test again indicates less evolution of damage up to 85% UCS, comparing to relaxation and creep.

4. DISCUSSION

4.1 Time- dependent Failure in Brittle Rocks

Brittle rocks subjected to time-dependent loading conditions are found to collapse under a lower stress level than their ultimate strength after a period of time. In practical conditions, various mechanisms could result in weakening of the rock mass over time such as creep, stress relaxation, consolidation/dilation or strength degradation depending upon the boundary conditions (Paraskevopoulou et al. 2018). In this study, multistage relaxation and creep experiments were conducted on brittle rocks and it was found that the damage evolution in rocks under multistage creep had a strong effect on the deformation behavior of the rock specimen as compared to relaxation and led to the failure of the rock specimen in a short resting period as compared to relaxation.

Figure 2c showed that in case of stress relaxation, the relaxation was more pronounced at stage ‘e’ as compared to the other stages. The AE and DIC results indicated higher evolution of damage at this stage in the rock specimen. This is because of the higher elastic modulus degradation at a stress level beyond the CD of the rock specimen. It is also evident from Figure 3d that during all the stages of stress relaxation except stage ‘e’ the cumulative number of AEs followed almost the same trend as the axial strain; however, the AE event rate and cumulative events showed a dramatic increase at stage ‘e’ (i.e., 85% of stress

relaxation) which can be associated with the macroscopic failure of the rock specimen. These results showed that at higher strain levels above CD, the specimen can fail even when stress decreases due to relaxation and it is just a matter of time that the cracks grow, coalesce and result in the failure of the specimen (Li and Xia 2000; Paraskevopoulou et al. 2018).

The AE source locations and their cracking mechanisms illustrated that a large number of tensile cracks were developed at stage ‘e’ of relaxation which than grow in an unstable manner and after a certain period of time, led to the failure of the specimen. To better understand the microstructural mechanisms (intragranular or transgranular) of the cracks produced in the relaxation period at different stages, other observational techniques like scanning electron microscopy (SEM) can be used.

Under multistage creep, as the loading time (creep stage) increased, the axial strain, AE event rate, and cumulative AE events increased. Since the AE signal was recorded, until the complete failure of the specimen, the amplitude of the events in all stages of creep were monitored. The amplitude and event rate of the AEs in case of creep were relatively higher than the relaxation, indicating faster damage evolution and less time to failure. At stage ‘e’ the high amplitude events are representative of large cracks causing the failure of the specimen. This explains why b-value in case of creep is lower than relaxation. Table 1 shows a comparison of the axial, lateral and volumetric strain variation along with the AE events generated at each stage of relaxation and creep. It is evident from Table 1 that the damage at each stress level in case of creep is much more than that in relaxation, especially the lateral strain variation caused by the extension of large number of microcracks in each stage.

Here a question arises ‘If we load the specimen at a stress level below the CD (in the stable crack growth period) and leave it for certain duration under creep and relaxation, will the rock actually fail in this condition? In case of relaxation under the dry condition, when the strain is held constant, no external energy is imposed on the specimen. The immediate effect is the stress relaxation due to crack propagation (Peng 1973). Once the crack growth stabilizes, the stress reaches an asymptotic value. To again initiate the cracking process, additional external energy is required and hence, failure is usually not observed in case of relaxation at a stress level below CD.

In case of creep in brittle rocks, under dry conditions, when the load is held constant at a stress level below the CD of the rock specimen, the secondary creep stage is not always observed and failure can still occur due to the accumulation of irreversible (plastic) strains with time, referred as the tertiary creep stage.

In addition to this, a different damage mechanism, known as stress corrosion may take place for time-dependent strength degradation in crystalline rocks in the presence of some external agent such as water or

any other agent (temperature, pressure or chemically active fluids). Stress corrosion is one of the dominant mechanisms responsible for time-dependent weakening of the brittle rocks. It is referred to as a chemical reaction between the strained bonds at the crack tips and the corrosive agent (such as water or gas), which eventually facilitates crack propagation (Atkinson and Meredith 1983) at a lower stress. The requirements for stress corrosion are: 1) existence of cracks, 2) tensile stress, 3) corrosive agent such as water or gas, and 4) time. Stress corrosion leads to the subcritical crack growth (Das and Scholz 1981; Atkinson 1984; Fairhurst et al. 2010), described as the growth of the cracks when the stress intensity factor is less than the fracture toughness of the material. Hence, the rock may fail at a lower stress level under stress relaxation and creep due to the growth of subcritical cracks as reported in several studies (Atkinson and Rawlings 1981; Miura et al. 2003; Ko and Kemeny 2013).

Few studies also show that if a rock is subjected to a stress level lower than or equal to CI, the rock does not fail even after long durations (Damjanac and Fairhurst 2010). In case of intact rock, Damjanac and Fairhurst (2010) have demonstrated that there is a stress threshold in the range of 40-60% of the UCS (greater than or equal to CI) which acts as a lower bound to the long-term strength of the rocks in confined as well as unconfined conditions. However, the response of brittle rocks with pre-existing flaws under such low stress levels of relaxation and creep remains to be explored. Hence, future studies involving long-term single stage relaxation and creep experiments on rocks with pre-existing flaws under lower levels of stress (lower than CI) and in the presence of water can provide valuable observations.

4.2 Implication for Field Applications

The work presented in this study can help with better understanding of the time-dependent behavior of rocks either when fracturing is a blessing or when it is a curse. The evolution of high number of cracks at lower stress level (85% of UCS) in long-term tests demonstrates its positive effects for fracturing in field applications such as EGS (Enhanced Geothermal System) in which a complex fracture network can be produced at a lower stress level with a lot of tensile cracks rather than high seismogenic shear cracks. Considering each AE as a proxy for a crack, the high number of AE hypocenters in case of relaxation and creep experiments can be correlated to a complex fracture network at a lower stress level. In addition, the higher b-value and relatively low amplitude events in case of relaxation indicated the evolution of low energy events, hence providing an explanation for a large number of tensile microcracks at a lower induced seismicity. These observations are very similar to the results obtained by hydraulic fracturing experiments on dry sandstone under cyclic injection (Patel et al. 2017). In their study, 16% reduction in the breakdown pressure was observed due to cyclic injection and a greater number of AE events were observed indicating increased damage around the hydraulic fracture.

Results of our study can also be linked to understand the time dependent properties of brittle rocks such as granite which serves as potential host rocks for nuclear waste repositories in which the desired lifetime is more than 1000 years. In this study, we have observed a reduction of 15% in three hours of relaxation and 30 minutes of creep under dry condition, eliminating all the extraneous factors contributing to the stress corrosion such as thermal fluctuations and fluids. However, in field conditions due to the existence of fluids and gas, the stress corrosion and subcritical crack growth could cause reduction of strength and failure of the rock even at a stress level lower than CD, considering that pre-existing discontinuities are also present in the field. Long-term relaxation and creep can increase the risk of early failure and therefore when designing these structures, the long-term behavior and the rheological properties of the rocks must be taken into account carefully.

5. CONCLUSIONS

This study focused on the time-dependent behavior of rocks under different levels of constant axial strain and constant axial stress. Specifically, multistage creep and relaxation laboratory experiments were conducted on Barre granite specimens under uniaxial compression loading. The results were analyzed using the AE monitoring and 2D-DIC strain measurement. Based on the observation, the main conclusions are summarized as follows:

(1) The laboratory results showed that the time to failure in case of creep is much less (~ 30 minutes) than that for relaxation (~ 2.5 hrs) when loaded above the CD threshold. The increased AEs and the volumetric strain distribution provided evidence for the formation of more microcracks and their coalescence at a lower stress level in the creep experiments as compared to the relaxation experiments. Failure occurred at 85% stress level in BG, reduction in strength (~15%) was less as compared to the sedimentary rocks (25~30%), indicating that BG possesses a less time-dependent property.

(2) Cumulative AE event and the event rate for multistage creep was higher than multistage relaxation. The spatial and temporal distribution of the AE sources decomposed into their mode of deformation illustrated the dominant behavior of the tensile cracking in the longer-term experiments compared to the shear and mixed mode cracks.

(3) The b-value for relaxation and creep experiments were estimated to identify the relative size distribution of the events. The higher b-value for the relaxation experiments indicated many low energy AE events generated throughout the experiment corresponding to less energy dissipation and slow crack growth, while a lower b-value for the creep experiment represented a faster and unstable crack growth accompanied by relatively higher amplitude AEs in large number. The

results suggest that b-value derived by the maximum likelihood method can be used as a precursor to macroscopic failure of the rock specimen in case of longer-term experiments.

This study illustrates that the specimen subjected to driving stress near or above the CD threshold can be expected to fail within few hours. The laboratory test results for relaxation experiments indicated that there is potential of increasing the fracture network at a lower stress level in the field even under strain-controlled loading schemes (i.e., multistage relaxation experiments). In future work, the results obtained through the multistage relaxation and creep experiments could be further compared with the long-term single-stage experiments to identify the effect of time on the fracture process and mechanisms. In addition, the energy partitioning needs to be done to characterize the proportion of the radiated seismic energy by the fractures produced under different time-dependent loading conditions. These findings can be applied to better understand the time-dependent processes occurring in Earth's brittle upper crust.

STATEMENTS AND DECLARATIONS

The authors declare that they have no competing financial interests or personal relationships that could have appeared to influence the work reported in this paper.

ACKNOWLEDGEMENTS

This research article is based upon the work supported by the U.S. Department of Energy, Office of Basic Energy Sciences, under Award Number DE-SC0019117. This support is gratefully acknowledged.

REFERENCES

1. Amitrano, D. (2003). Brittle-ductile transition and associated seismicity: Experimental and numerical studies and relationship with the b value. *Journal of Geophysical Research: Solid Earth*, 108(B1).
2. Atkinson, B. K. (1984). Subcritical crack growth in geological materials. *Journal of Geophysical Research: Solid Earth*, 89(B6), 4077-4114.
3. Atkinson, B. K., & Rawlings, R. D. (1981). Acoustic emission during stress corrosion cracking in rocks. *Earthquake prediction: An international review*, 4, 605-616.
4. Baptista-Pereira, C. & Goncalves da Silva, B. (2019). Effects of fluid diffusivity on hydraulic fracturing processes using visual analysis. In *53rd US Rock Mechanics/Geomechanics Symposium*, OnePetro, June 2019.
5. Bieniawski, Z. T. (1967). Mechanism of brittle fracture of rock: part I—theory of the fracture process. In *International Journal of Rock Mechanics and Mining Sciences & Geomechanics Abstracts* (Vol. 4, pp. 395-406).
6. Brantut, N., Heap, M. J., Meredith, P. G., & Baud, P. (2013). Time-dependent cracking and brittle creep in crustal rocks: A review. *Journal of Structural Geology*, 52, 17-43.
7. Dai, F. & Xia, K. (2010). Loading rate dependence of tensile strength anisotropy of Barre granite. *Pure and Applied Geophysics*, 167(11), 1419-1432.
8. Damjanac, B., & Fairhurst, C. (2010). Evidence for a long-term strength threshold in crystalline rock. *Rock Mechanics and Rock Engineering*, 43(5), 513-531.

9. Das, S., & Scholz, C. H. (1981). Theory of time-dependent rupture in the Earth. *Journal of Geophysical Research: Solid Earth*, 86(B7), 6039-6051.

10. Diederichs, M. S. (2003). Manuel Rocha medal recipient rock fracture and collapse under low confinement conditions. *Rock Mechanics and Rock Engineering*, 36(5), 339-381.

11. Diederichs, M. S., Kaiser, P. K., & Eberhardt, E. (2004). Damage initiation and propagation in hard rock during tunnelling and the influence of near-face stress rotation. *International Journal of Rock Mechanics and Mining Sciences*, 41(5), 785-812.

12. Diederichs, M. S. & Kaiser, P. K. (1999). Tensile strength and abutment relaxation as failure control mechanisms in underground excavations. *International Journal of Rock Mechanics and Mining Sciences*, 36(1), 69-96.

13. Eberhardt, E., Stead, D., Stimpson, B., & Read, R. S. (1998). Changes in acoustic event properties with progressive fracture damage. *International Journal of Rock Mechanics and Mining Sciences*, 34(3-4), 71-e1.

14. Einstein, H. H. (1996). Tunnelling in difficult ground—swelling behaviour and identification of swelling rocks. Rock mechanics and rock engineering, 29(3), 113-124.

15. Farahmand, K. & Diederichs, M. S. (2015). A calibrated synthetic rock mass (SRM) model for simulating crack growth in granitic rock considering grain scale heterogeneity of polycrystalline rock. In *49th US Rock Mechanics/Geomechanics Symposium*. American Rock Mechanics Association, November 2015.

16. Ghazvinian, E. (2015). Fracture initiation and propagation in low porosity crystalline rocks: Implications for excavation damage zone (EDZ) mechanics (doctoral dissertation).

17. Goebel, T. H.W., Schorlemmer, D., Becker, T. W., Dresen, G., & Sammis, C. G. (2013). Acoustic emissions document stress changes over many seismic cycles in stick-slip experiments. *Geophysical Research Letters*, 40(10), 2049-2054.

18. Gdoutos, E. E. (2005). *Fracture Mechanics* (Vol # 123). Springer.

19. Gutenberg, B., & Richter, C. F. (1944). Frequency of earthquakes in California. *Bulletin of the Seismological society of America*, 34(4), 185-188.

20. Heap, M. J., Baud, P., Meredith, P. G., Bell, A. F., & Main, I. G. (2009). Time-dependent brittle creep in Darley Dale sandstone. *Journal of Geophysical Research: Solid Earth*, 114(B7).

21. Hedayat, A., Pyrak-Nolte, L. J., & Bobet, A. (2014). Detection and quantification of slip along non-uniform frictional discontinuities using digital image correlation. Geotechnical Testing Journal, 37(5), 786-799.

22. Hudson, J. A. & Harrison, J. P. (2000). *Engineering Rock Mechanics: An Introduction to the Principles*. Elsevier.

23. Innocente, J. C., Paraskevopoulou, C., & Diederichs, M. S. (2021). Estimating the long-term strength and time-to-failure of brittle rocks from laboratory testing. *International Journal of Rock Mechanics and Mining Sciences*, 147, 104900.

24. Iqbal, M. & Mohanty, B. (2007). Experimental calibration of ISRM suggested fracture toughness measurement techniques in selected brittle rocks. *Rock Mechanics and Rock Engineering*, 40 (5), 453.

25. Kaiser, P. K., Diederichs, M. S., Martin, C. D., Sharp, J., & Steiner, W. (2000). Underground works in hard rock tunnelling and mining. In *ISRM international symposium*, OnePetro, November 2000.

26. Kemeny, J. (2005). Time-dependent drift degradation due to the progressive failure of rock bridges along discontinuities. *International Journal of Rock Mechanics and Mining Sciences*, 42(1), 35-46.

27. Kranz, R. L. (1983). Microcracks in rocks: a review. *Tectonophysics*, 100 (1-3), 449–480.

28. Ko, T. Y., & Kemeny, J. (2007). Effect of confining stress and loading rate on fracture toughness of rocks. In *1st Canada-US Rock Mechanics Symposium*. OnePetro, May 2007.

29. Lajtai, E. Z. (1974). Brittle fracture in compression. *International Journal of Fracture*, 10(4), 525-536.

30. Lei, X. (2003). How do asperities fracture? An experimental study of unbroken asperities. *Earth and Planetary Science Letters*, 213(3-4), 347-359.

31. Li, B. Q., da Silva, B. G., & Einstein, H. (2019). Laboratory hydraulic fracturing of granite: Acoustic emission observations and interpretation. *Engineering Fracture Mechanics*, 209, 200-220.

32. Li, Y. & Xia, C. (2000). Time-dependent tests on intact rocks in uniaxial compression. *International Journal of Rock Mechanics and Mining Sciences*, 37(3), 467-475.

33. Li, B. Q., da Silva, B. G., & Einstein, H. (2019). Laboratory hydraulic fracturing of granite: Acoustic emission observations and interpretation. *Engineering Fracture Mechanics*, 209, 200-220.

34. Liu, J., Yang, H., Xiao, Y., & Zhou, X. (2018). Macro-mesoscopic fracture and strength character of pre-cracked granite under stress relaxation condition. *Rock Mechanics and Rock Engineering*, 51(5), 1401-1412.

35. Liu, Y., Liu, C., Kang, Y., Wang, D., & Ye, D. (2015). Experimental research on creep properties of limestone under fluid–solid coupling. *Environmental Earth Sciences*, 73(11), 7011-7018.

36. Main, I. G., Meredith, P. G., & Jones, C. (1989). A reinterpretation of the precursory seismic b-value anomaly from fracture mechanics. *Geophysical Journal International*, 96(1), 131-138.

37. Malan, D. F. (2002). Manuel Rocha medal recipient simulating the time-dependent behaviour of excavations in hard rock. Rock Mechanics and Rock Engineering, 35(4), 225-254.

38. Martin, C. D. & Chandler, N. A. (1994). The progressive fracture of Lac du Bonnet granite. In *International Journal of Rock Mechanics and Mining Sciences and Geomechanics Abstracts* (Vol. 31, No. 6, pp. 643-659). Pergamon.

39. MATSUSHIMA, S. (1960). On the flow and fracture of igneous rocks. *Bulletins-Disaster Prevention Research Institute*, Kyoto University, 36, 1-9.

40. McLaskey, G. C. & Lockner, D. A. (2014). Preslip and cascade processes initiating laboratory stick slip. *Journal of Geophysical Research: Solid Earth*, 119(8), 6323-6336.

41. Meredith, P. G., Main, I. G., & Jones, C. (1990). Temporal variations in seismicity during quasi-static and dynamic rock failure. *Tectonophysics*, 175(1-3), 249-268.

42. Meredith, P. G., & Atkinson, B. K. (1983). Stress corrosion and acoustic emission during tensile crack propagation in Whin Sill dolerite and other basic rocks. *Geophysical Journal International*, 75(1), 1-21.

43. Mishra, B. & Verma, P. (2015). Uniaxial and triaxial single and multistage creep tests on coal-measure shale rocks. *International Journal of Coal Geology*, 137, 55-65.

44. Miura, K., Okui, Y., & Horii, H. (2003). Micromechanics-based prediction of creep failure of hard rock for long-term safety of high-level radioactive waste disposal system. *Mechanics of Materials*, 35(3-6), 587-601.

45. Mogi, K. (1963). Magnitude-frequency relation for elastic shocks accompanying fractures of various materials and some related problems in earthquakes (2nd paper). *Bulletin of the Earthquake Research Institute, University of Tokyo*, 40(4), 831-853.

46. Moore, D. E. & Lockner, D. A. (1995). The role of microcracking in shear-fracture propagation in granite. *Journal of Structural Geology*, 17(1), 95-114.

47. Moradian, Z., Einstein, H. H., & Ballivy, G. (2016). Detection of cracking levels in brittle rocks by parametric analysis of the acoustic emission signals. *Rock Mechanics and Rock Engineering*, 49 (3), 785–800.

48. Morgan, S. P., Johnson, C. A., & Einstein, H. H. (2013). Cracking processes in Barre granite: fracture process zones and crack coalescence. *International Journal of Fracture* 180 (2), 177–204.

49. Munoz, H., Taheri, A., & Chanda, E. K. (2016). Pre-peak and post-peak rock strain characteristics during uniaxial compression by 3D digital image correlation. *Rock Mechanics and Rock Engineering*, 49(7), 2541-2554.

50. Munoz, H., & Taheri, A. (2018). Postpeak deformability parameters of localized and nonlocalized damage zones of rocks under cyclic loading. *ASTM International*.

51. Nara, Y., Takada, M., Mori, D., Owada, H., Yoneda, T., & Kaneko, K. (2010). Subcritical crack growth and long-term strength in rock and cementitious material. *International Journal of Fracture*, 164(1), 57-71.

52. Nasseri, M., Grasselli, G., & Mohanty, B. (2010). Fracture toughness and fracture roughness in anisotropic granitic rocks. *Rock Mechanics and Rock Engineering*, 43 (4), 403–415.

53. Nicksiar, M., & Martin, C. D. (2012). Evaluation of methods for determining crack initiation in compression tests on low-porosity rocks. *Rock mechanics and Rock engineering*, 45(4), 607-617.

54. Nicksiar, M. & Martin, C. D. (2013). Crack initiation stress in low porosity crystalline and sedimentary rocks. *Engineering Geology*, 154, 64-76.

55. ÖZSEN, H., Özkan, İ., & SENSÖGÜT, C. (2014). Measurement and mathematical modelling of the creep behaviour of Tuzköy rock salt. *International Journal of Rock Mechanics and Mining Sciences* (1997), 66, 128-135.

56. Pramthawee, P., Jongpradist, P., & Sukkarak, R. (2017). Integration of creep into a modified hardening soil model for time-dependent analysis of a high rockfill dam. *Computers and Geotechnics*, 91, 104-116.

57. Paraschiv-Munteanu, I., & Cristescu, N. D. (2001). Stress relaxation during creep of rocks around deep boreholes. *International Journal of Engineering Science*, 39(7), 737-754.

58. Paraskevopoulou, C., Perras, M., Diederichs, M., Amann, F., Löw, S., Lam, T., & Jensen, M. (2017). The three stages of stress relaxation-Observations for the time-dependent behavior of brittle rocks based on laboratory testing. *Engineering Geology*, 216, 56-75.

59. Paraskevopoulou, C., Perras, M., Diederichs, M., Loew, S., Lam, T., & Jensen, M. (2018). Time-dependent behaviour of brittle rocks based on static load laboratory tests. *Geotechnical and Geological Engineering*, 36(1), 337-376.

60. Patel, S. M., Sondergeld, C. H., & Rai, C. S. (2017). Laboratory studies of hydraulic fracturing by cyclic injection. *International Journal of Rock Mechanics and Mining Sciences*, 95, 8-15.

61. Peng, S. & Podnieks, E. R. (1972). Relaxation and the behavior of failed rock. In *International Journal of Rock Mechanics and Mining Sciences & Geomechanics Abstracts* (Vol. 9, No. 6, pp. 699-700). Pergamon.

62. Peng, S. S. (1973). Time-dependent aspects of rock behavior as measured by a servocontrolled hydraulic testing machine. In *International Journal of Rock Mechanics and Mining Sciences & Geomechanics Abstracts* (Vol. 10, No. 3, pp. 235-246). Pergamon.

63. Qu, H., Wu, X., Huang, P., Tang, S., Wang, R., & Hu, Y. (2022). Acoustic Emission and Failure Characteristics of Shales with Different Brittleness Under AWJ Impingement. *Rock Mechanics and Rock Engineering*, 1-16.

64. Rao, M. V. M. S., & Lakshmi, K. P. (2005). Analysis of b-value and improved b-value of acoustic emissions accompanying rock fracture. *Current science*, 1577-1582.

65. Rivière, J., Lv, Z., Johnson, P. A., & Marone, C. (2018). Evolution of b-value during the seismic cycle: Insights from laboratory experiments on simulated faults. *Earth and Planetary Science Letters*, 482, 407-413.

66. Sammonds, P., & Ohnaka, M. (1998). Evolution of microseismicity during frictional sliding. *Geophysical Research Letters*, 25(5), 699-702.

67. Lennartz-Sassinek, S., Main, I. G., Zaiser, M., & Graham, C. C. (2014). Acceleration and localization of subcritical crack growth in a natural composite material. *Physical Review E*, 90(5), 052401.

68. Rydelek, P. A., & Sacks, I. S. (1989). Testing the completeness of earthquake catalogues and the hypothesis of self-similarity. *Nature*, 337(6204), 251-253.

69. Scholz, C. H. (2015). On the stress dependence of the earthquake b value. *Geophysical Research Letters*, 42(5), 1399-1402.

70. Schulze, O. (2011). Strengthening and stress relaxation of Opalinus clay. *Physics and Chemistry of the Earth, Parts A/B/C*, 36(17-18), 1891-1897.

71. Shirole, D., Hedayat, A., & Walton, G. (2019). Experimental relationship between compressional wave attenuation and surface strains in brittle rock. *Journal of Geophysical Research: Solid Earth*, 124(6), 5770-5793.

72. Shirole, D., Hedayat, A., & Walton, G. (2020). Illumination of damage in intact rocks by ultrasonic transmission-reflection and digital image correlation. *Journal of Geophysical Research: Solid Earth*, 125(7), e2020JB019526.

73. Shirole, D., Walton, G., & Hedayat, A. (2020). Experimental investigation of multi-scale strain-field heterogeneity in rocks. *International Journal of Rock Mechanics and Mining Sciences*, 127, 104212.

74. Singh, D. P. (1975, September). A study of creep of rocks. *In International Journal of Rock Mechanics and Mining Sciences & Geomechanics Abstracts* 12(9), 271-276.

75. Sutton, M. A., Orteu, J. J., & Schreier, H. (2009). Image *Correlation for Shape, Motion, and Deformation Measurements: Basic Concepts, Theory, and Applications*. Springer Science & Business Media.

76. Tapponnier, P. & Brace, W. F. (1976). Development of stress-induced microcracks in Westerly granite. In *International Journal of Rock Mechanics and Mining Sciences & Geomechanics Abstracts* (Vol. 13, No. 4, pp. 103-112). Pergamon.

77. Tian, H. M., Chen, W., Tian, T. I. A. N., Wang, H., & Zhao, W. (2012). Experimental and theoretical studies of creep damage behavior of soft rock. Chinese Journal of Rock Mechanics and Engineering, 31(3), 610-617.

78. Tian, H. M., Chen, W. Z., Yang, D. S., & Gong, Z. (2015). Experimental and numerical analysis of the time-dependent behavior of argillaceous red sandstone under high in situ stress. *Bulletin of Engineering Geology and the Environment*, 74(2), 567-575.

79. Tian, H., Chen, W., Yang, D., & Dai, F. (2016). Relaxation behavior of argillaceous sandstone under high confining pressure. *International Journal of Rock Mechanics and Mining Sciences*, (88), 151-156.

80. W. Goebel, T. H., Schorlemmer, D., Becker, T. W., Dresen, G., & Sammis, C. G. (2013). Acoustic emissions document stress changes over many seismic cycles in stick-slip experiments. *Geophysical Research Letters*, 40(10), 2049-2054.

81. Wang, R., Li, L., & Simon, R. (2019). A model for describing and predicting the creep strain of rocks from the primary to the tertiary stage. *International Journal of Rock Mechanics and Mining Sciences*, 123, 104087.

82. Wang, Z., Gu, L., Shen, M., Zhang, F., Zhang, G., & Wang, X. (2019). Shear stress relaxation behavior of rock discontinuities with different joint roughness coefficient and stress histories. *Journal of Structural Geology*, 126, 272-285.

83. Woessner, J., & Wiemer, S. (2005). Assessing the quality of earthquake catalogues: Estimating the magnitude of completeness and its uncertainty. *Bulletin of the Seismological Society of America*, 95(2), 684-698.

84. Wyss, M., & Wiemer, S. (2000). Change in the probability for earthquakes in southern California due to the Landers magnitude 7.3 earthquake. *Science*, 290(5495), 1334-1338.

85. Xu, T., Tang, C. A., Zhao, J., Li, L., & Heap, M. J. (2012). Modelling the time-dependent rheological behavior of heterogeneous brittle rocks. *Geophysical Journal International*, 189(3), 1781-1796.

86. Yang, X. J. (2017). New general fractional-order rheological models with kernels of Mittag-Leffler functions. *Romanian Reports in Physics*, 69(4), 118.

87. Yu, H., Li, Y., & Liu, H. (2012). Comparative study of conventional mechanical, creep and stress relaxation properties of silty mudstone under triaxial compression. *Chinese Journal of Rock Mechanics and Engineering*, 31(1), 60-70.

88. Yu, J., Liu, G., Cai, Y., Zhou, J., Liu, S., & Tu, B. (2020). Time-dependent deformation mechanism for swelling soft-rock tunnels in coal mines and its mathematical deduction. *International Journal of Geomechanics*, 20(3), 04019186.

89. Zafar, S., Hedayat, A., & Moradian, O. (2020). Evaluation of crack initiation and damage in intact barre granite rocks using acoustic emission. *Geotechnical Earthquake Engineering and Special Topics*.

90. Zafar, S., Hedayat, A., & Moradian, O. (2022). Evolution of Tensile and Shear Cracking in Crystalline Rocks Under Compression. *Theoretical and Applied Fracture Mechanics*, 103254.

91. Zang, A., Christian Wagner, F., Stanchits, S., Dresen, G., Andresen, R., & Haidekker, M. A. (1998). Source analysis of acoustic emissions in Aue granite cores under symmetric and asymmetric compressive loads. *Geophysical Journal International*, 135(3), 1113-1130.

92. Zhang, Y., Xu, W. Y., Gu, J. J., & Wang, W. (2013). Triaxial creep tests of weak sandstone from fracture zone of high dam foundation. *Journal of Central South University*, 20(9), 2528-2536.

93. Zhang, Y., Zhang, Z., Xue, S., Wang, R., & Xiao, M. (2020). Stability analysis of a typical landslide mass in the Three Gorges Reservoir under varying reservoir water levels. *Environmental Earth Sciences*, 79(1), 1-14.

94. Zhao, K., Yang, D., Zeng, P., Gong, C., Wang, X., & Zhong, W. (2021). Accelerating creep stage of red sandstone expressed and quantitatively identified based on acoustic emission information. *Rock Mechanics and Rock Engineering*, 54(9), 4867-4888.

95. Zhuang, L., Jung, S. G., Diaz, M., Kim, K. Y., Hofmann, H., Min, K. B., & Yoon, J. S. (2020). Laboratory true triaxial hydraulic fracturing of granite under six fluid injection schemes and grain-scale fracture observations. *Rock Mechanics and Rock Engineering*, 53(10), 4329-4344.

List of Figures

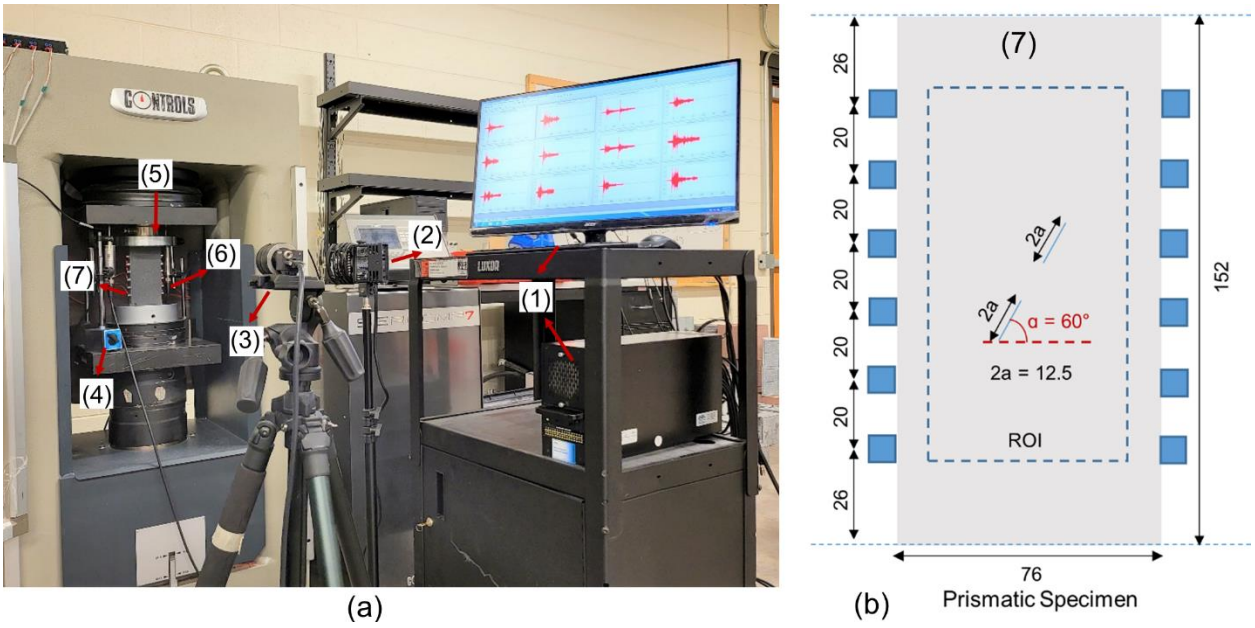

Fig. 1 Experimental setup for AE monitoring and 2D-DIC procedures: (a) (1) AE monitoring system, (2) lighting system for DIC, (3) CCD camera, (4) Linear variable differential transformer (LVDT), (5) Load cell, (6) Nano 30 AE sensors, (7) Barre granite specimen; (b) Speckled Barre granite specimen, small boxes denote the position of the AE transducers, the dotted line represents the ROI, flaw length is 12.5 mm and flaw inclination angle is 60° (all the dimensions are in mm).

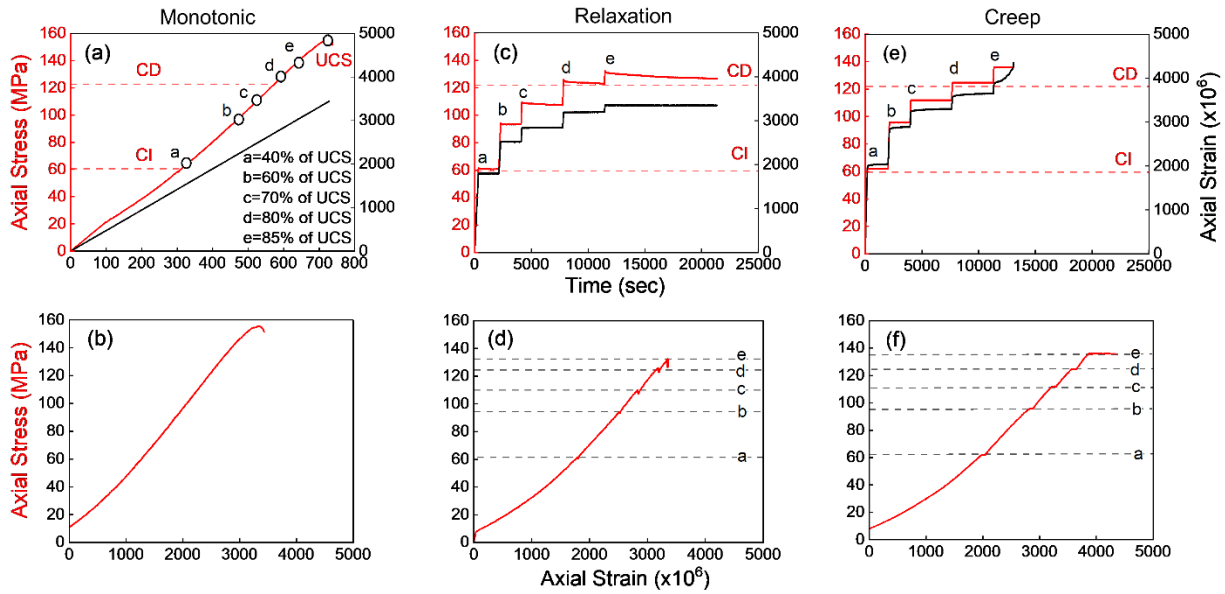

Fig. 2 (a) Stages of fracturing in brittle rocks (where: CI-crack initiation, CD-crack damage, UCS- unconfined compressive strength); (b) Stress-strain response under monotonic loading for specimen BG-2; (c) Axial stress and axial strain variation with the relaxation time expressed in seconds; (d) Stress-strain behavior under multistage relaxation for specimen MS-2; (e) Stress and axial strain variation for the creep experiments as a function of time for specimen MC-1; (f) Stress-strain response of Barre granite under multistage creep.

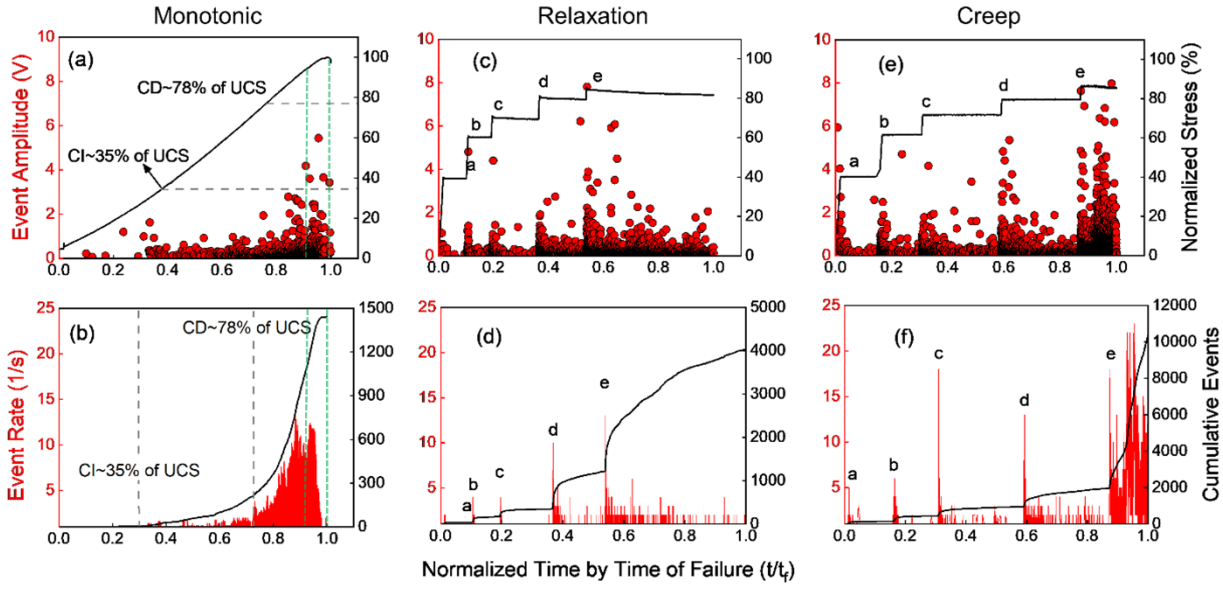

Fig. 3 Determination of the damage stress thresholds (CI and CD) from the monotonic experiments by the (a) AE event amplitude; (b) AE event rate and cumulative events for specimen BG-2 (Green inset represents the region where AE system showed some amplitude distortion due to clipping); (c) AE event amplitude corresponding to each stress level in case of relaxation; (d) Event rate and cumulative events corresponding to

relaxation at different stages; (e) AE event amplitude in case of multistage creep; (f) Event rate and cumulative events corresponding to each stress level in multistage creep.

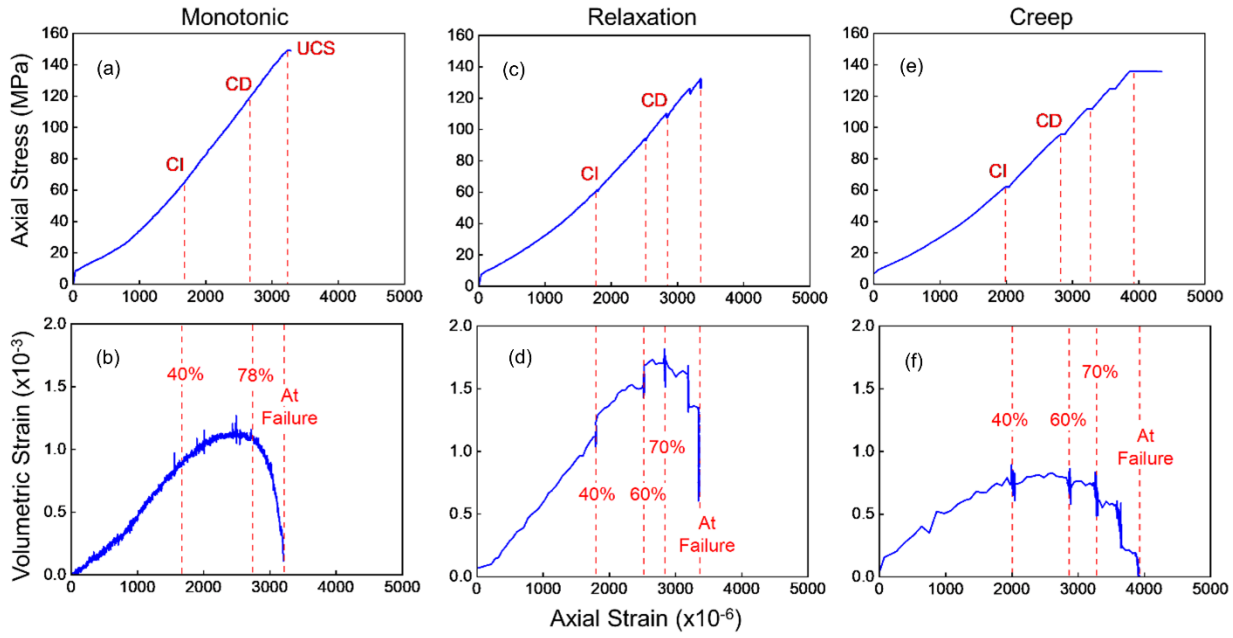

Fig. 4 Crack evolution process and corresponding volumetric strain curves for (a) & (b) Monotonic loading experiments; (c) & (d) Multistage relaxation experiments and (e) & (f) Multistage creep experiments.

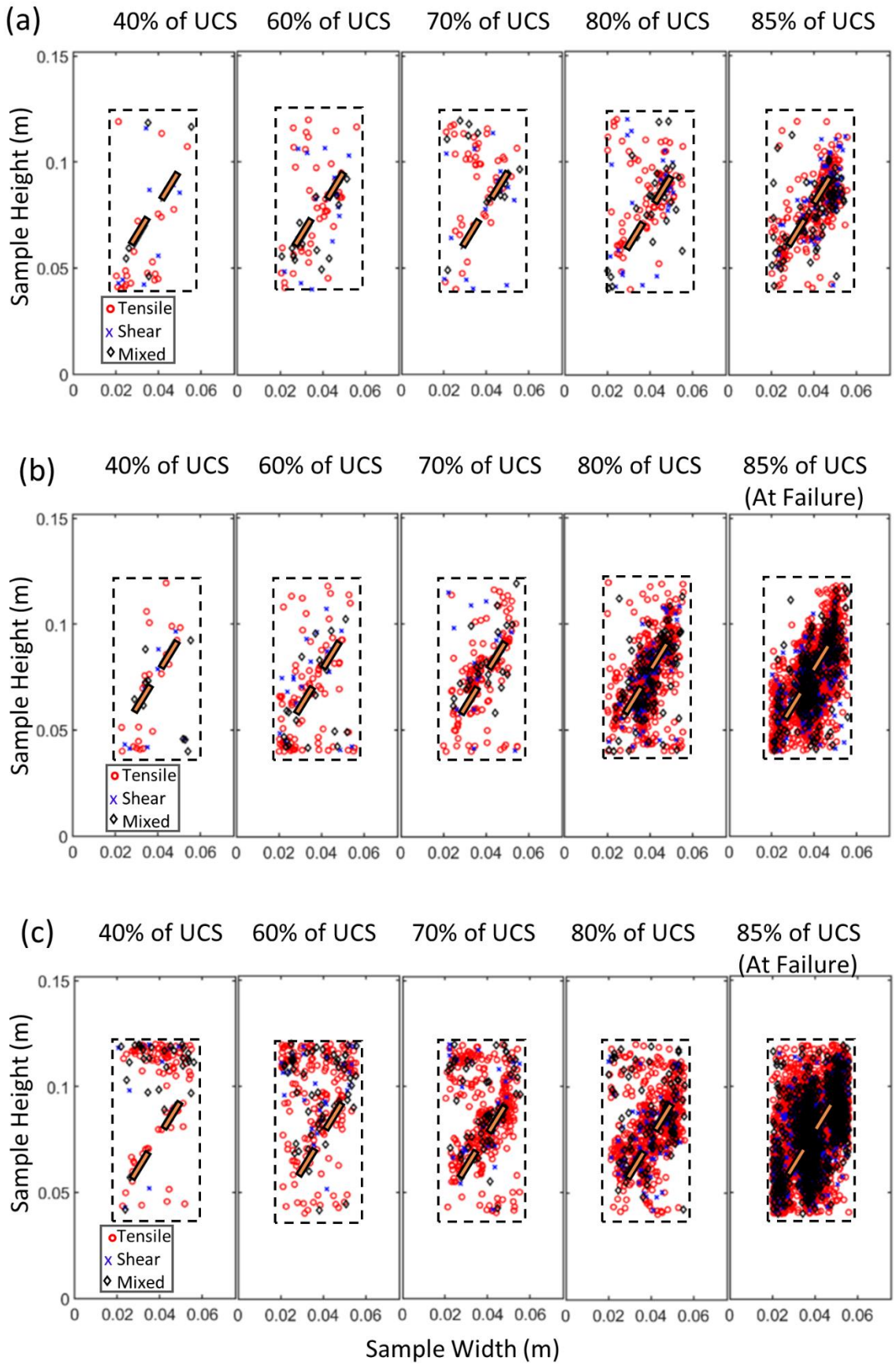
(a)
40% of UCS
60% of UCS
70% of UCS
80% of UCS
85% of UCS
Sample Height (m)
0.15
0.1
0.05
0
Tensile
Shear
Mixed
0
0.02
0.04
0.06
(b)
40% of UCS
60% of UCS
70% of UCS
80% of UCS
85% of UCS
(At Failure)
Sample Height (m)
Tensile
Shear
Mixed
(c)
40% of UCS
60% of UCS
70% of UCS
80% of UCS
85% of UCS
(At Failure)
Sample Height (m)
Tensile
Shear
Mixed
Sample Width (m)

Fig. 5 Spatial distribution of the AE hypocenters at different stress levels for (a) monotonic experiments; (b) multistage relaxation and (c) multistage creep experiments.

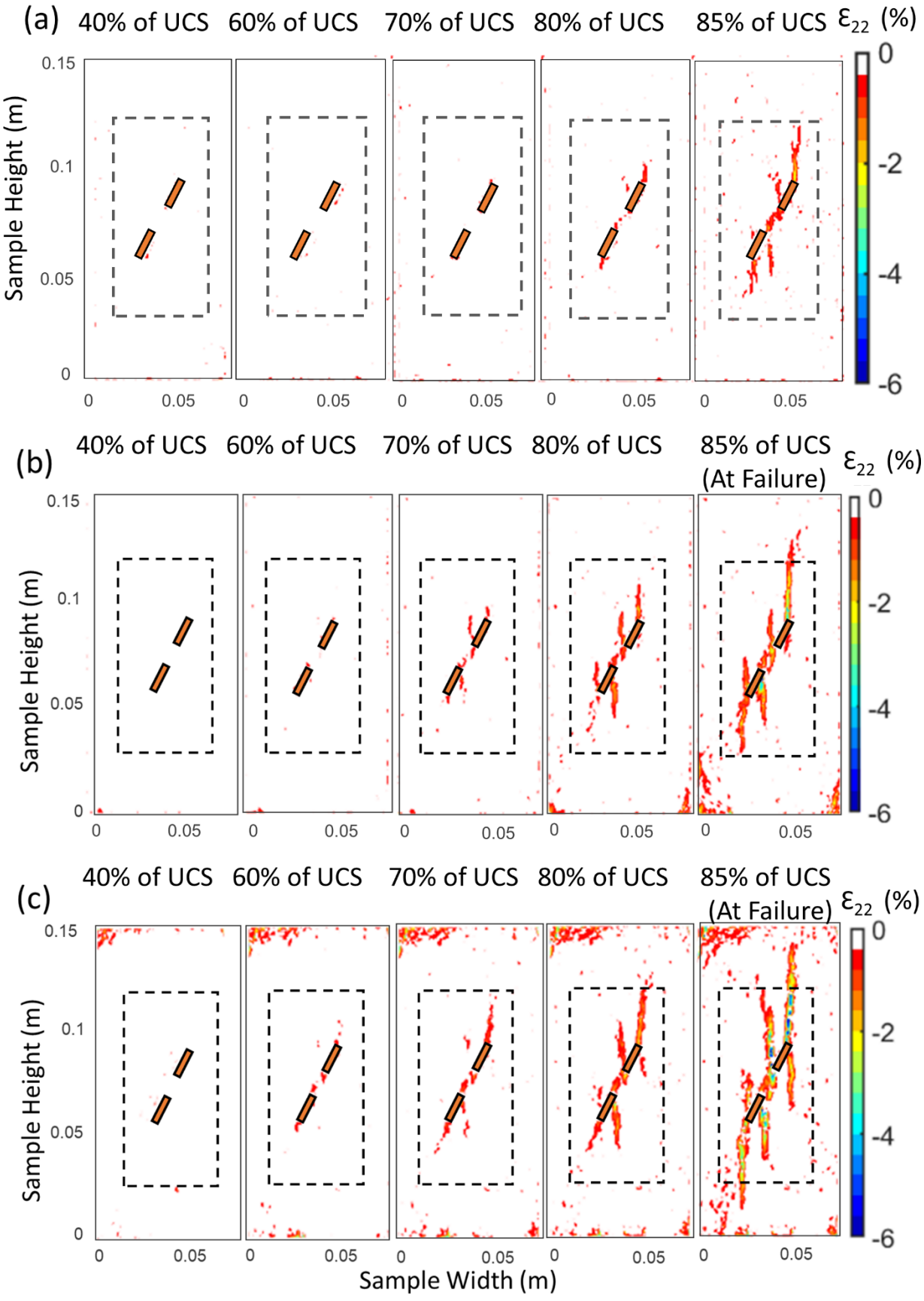
(a)
40% of UCS
60% of UCS
70% of UCS
80% of UCS
85% of UCS
ε22 (%)
Sample Height (m)
0.15
0.1
0.05
0
0
0.05
0
-2
-4
-6
(b)
40% of UCS
60% of UCS
70% of UCS
80% of UCS
85% of UCS
(At Failure)
ε22 (%)
Sample Height (m)
(c)
40% of UCS
60% of UCS
70% of UCS
80% of UCS
85% of UCS
(At Failure)
ε22 (%)
Sample Height (m)
Sample Width (m)

Fig. 6 Minor principal strain (ε_{22}; negative (-) represents extension) profile at different stress levels for (a) monotonic loading experiments; (b) Multistage relaxation experiments and (c) Multistage creep experiments.

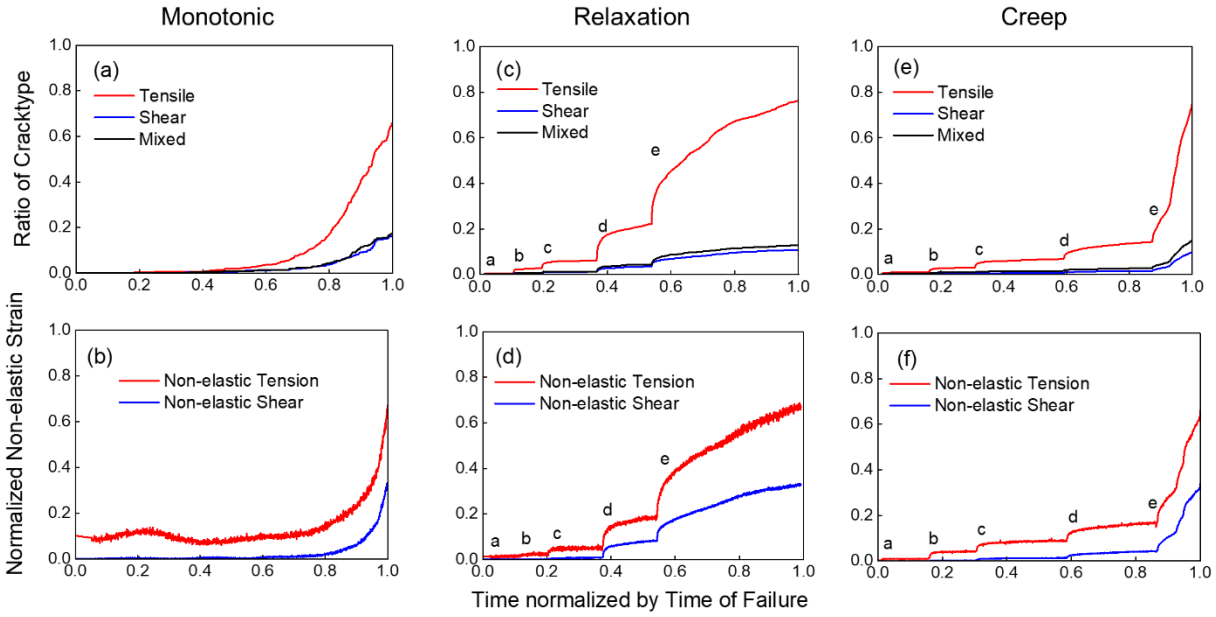

Fig. 7 Temporal evolution of different type of cracks for monotonic loading experiment obtained through (a) moment tensor inversion; (b) DIC analysis; for the relaxation experiments obtained through (c) moment tensor inversion; (b) DIC analysis; for the multistage creep experiments through (e) moment tensor inversion; (f) DIC analysis.

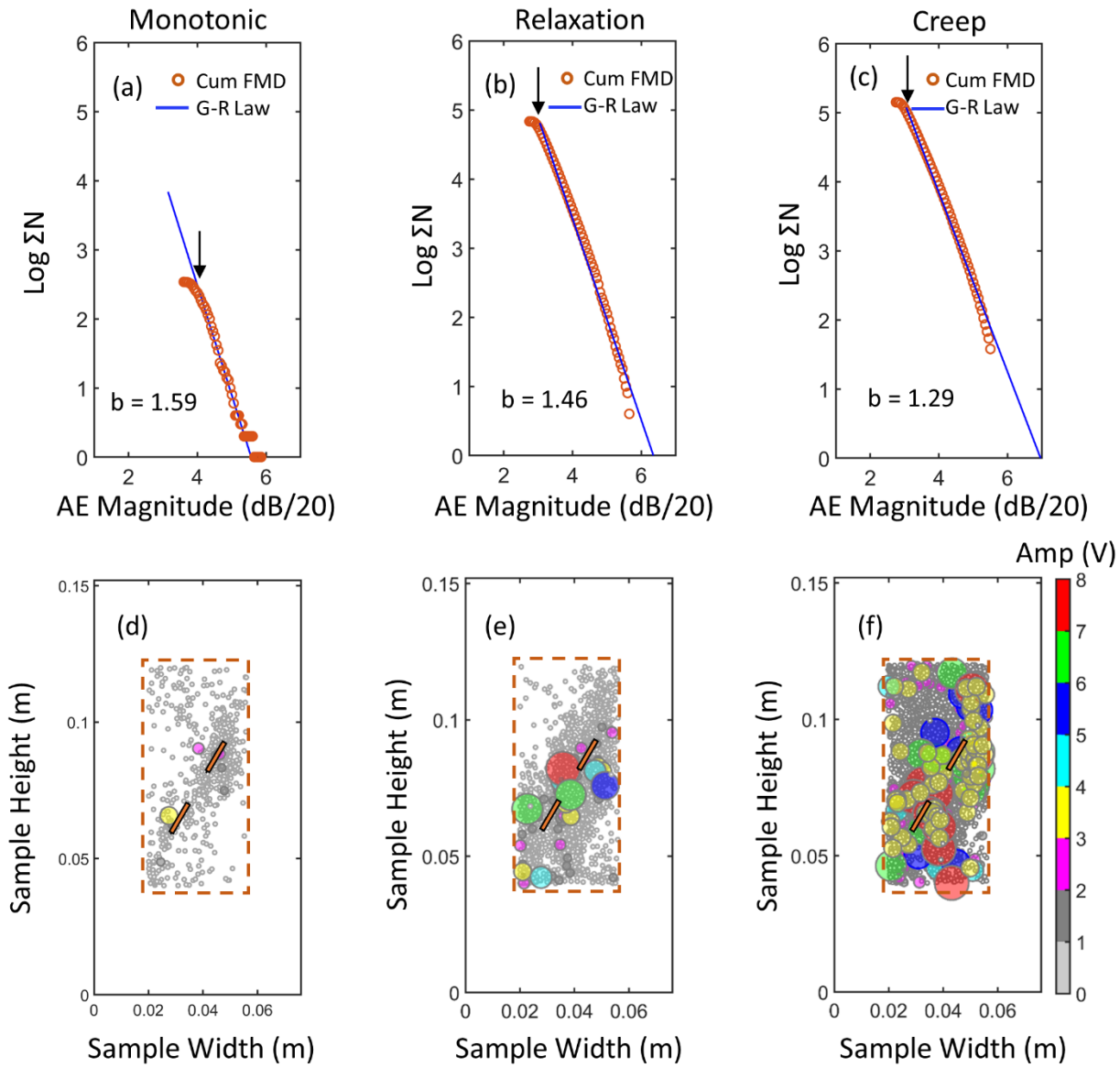

Fig. 8 Frequency-magnitude distribution of the events generated in (a) monotonic uniaxial experiments for specimen BG-2; (b) multistage relaxation experiments for specimen MS-2; and (c) multistage creep experiments for specimen MC-1. The bottom row illustrates the location of the events generated in (d) monotonic loading; (e) multistage relaxation experiments and (f) multistage creep experiments, size of the circles and colorbar denotes the amplitude of the events produced. Note the monotonic experiment results are up to 85% of UCS which is the corresponding stress level for failure in multistage relaxation and creep experiments.

List of Tables

Table 1. Strain and cumulative AE events for different loading stages in relaxation and creep. Negative (-) strain represents extension

Loading Stage	Normalized Axial Stress (%)	Axial Strain (με)		Lateral Strain (με)		Volumetric Strain (με)		AE events in each stage	
		Rel.	Creep	Rel.	Creep	Rel.	Creep	Rel.	Creep
a	40	1795	1988	-380	-689	1035	610	10	53
b	60	2523	2820	-538	-1120	1448	579	67	217
c	70	2831	3216	-171	-1366	1513	485	138	437
d	80	3183	3558	-659	-1661	1314	235	697	887
e	85	3352	3867	-1374	-2748	604	-1630	2769	8120